Computational and Experimental Studies on the CO_2 Adsorption of layered double hydroxide intercalated by anionic surfactant

Qiuping Liu[a],Yu Zhao[a], Zhe Jiang[a],Yanhong Cui[a], Jiawei Wang [c], Ning Ai[a,b,*]

[a] *College of Chemical Engineering, Zhejiang University of Technology, Hangzhou, China*

[b] *Zhejiang province key laboratory of biomass fuel, Hangzhou, China*

[c] *European Bioenergy Research Institute, Aston University, Birmingham, B4 7ET, United Kingdom*

Abstract

The Mg-Al, Ca-Al, Zn-Al and Mg-Fe layered double hydroxides intercalated by sodium dodecyl sulfate was prepared by a co-precipitation method. These materials were characterized by elemental analysis, Powder X-ray diffraction (XRD) and N_2 physical adsorption and desorption. Adsorption of CO_2 on the samples was investigated by thermogravimetric analysis at 30°C under 1 bar. The samples had a CO_2 adsorption capacity in the range of 0.35-0.58 mmol/g. Ca-Al layered double hydroxide intercalated by sodium dodecyl sulfate (SDS) had the highest CO_2 adsorption capacity. The layered structures were analyzed by using quantum chemical calculation methods. The simulation results showed that CO_2 adsorption capacity was correlated to the E_{LUMO} and the density of Lowest Unoccupied Molecular Orbital (LUMO). The higher E_{LUMO} and density of LUMO orbitals promoted the formation of O-H...O hydrogen bonds, which leaded to the higher CO_2 adsorption capacity.

Keywords: Layered Double Hydroxide, Carbon Capture, Adsorption, Quantum Chemical Calculation

*** Corresponding author.** E-mail:aining@zjut.edu.cn.

This work was supported by Zhejiang Provincial Natural Science Foundation of China（LY16B060014）

and State Key Laboratory of Chemical Engineering（No. SKL-ChE-08A01）

1. Introduction

CO_2 concentration in the atmospheric has been increasing rapidly, due to the combustion of fossil fuels in the recent years, which caused global warming (Aschenbrenner et al., 2011). The capture of CO_2 from various emission sources was considered an effective way to stabilize or decrease the CO_2 concentration (Hutson and Attwood, 2008; Zhao et al.,2012). Many synthetic and natural materials, such as mesoporous silicas (Zhao et al., 2012; Oliveira et al., 2018), zeolites (Hudson er al.,2012), activated carbons (Plaza et al., 2010), calcium and magnesium oxides (Liu et al., 2013), and hydrotalcites (Sharma et al., 2008), were considered to be adsorbents.

Layered double hydroxides (LDH), also known as hydrotalcite-like compounds or synthetic anionic clays, consist of positively charged layers and interlayer anions. The general formula of LDH is [M2+ 1-xM3+ $X(OH)_2]^{x+}$An- $x/n \cdot mH_2O$, where M^{2+} is the divalent metal cation, can be Mg^{2+}, Zn^{2+}, Ca^{2+}, Ni^{2+}, and M^{3+},which is the trivalent metal cation, can be Al^{3+}, Fe^{3+}, Cr^{3+}, Ga^{3+}, and A^{n-} can be OH^-, CO_3^{2-}, NO_3^-, Cl^-, SO_4^{2-}. The value of x was typically between 0.17 and 0.33 (Cavani et al., 1991). These materials could be readily synthesized and used as heterogeneous catalysts, ion exchangers, biomedical application, and heat stabilizers (Cavani et al., 1991; Bergaya et al., 2006).

Most of reports pay attention to the calcined materials of LDH at 400-600 ℃, because the mixed metal oxides, which calcined by LDH, had relatively large specific surface areas and high CO_2 adsorption capacity at elevated temperatures (Reddy et al., 2008; Zou et al., 2001; Ye and Abdullah, 2009; Wang et al., 2008; Wang et al., 2011). However, only few reports had focused on the pristine hydrotalcites as CO_2 adsorbents because of their low CO_2 adsorption capability (Aschenbrenner et al.,

2011; Torres-Rodríguez et al., 2011).

The materials structure had an influence on the adsorption capacity of LDH, which is further determined by synthetic parameters (Sharma et al., 2008). The CO_2 adsorption capacity of Mg-Al-CO_3 LDH could reach 8-22 cm^3/g at 30°C under 1 bar, which could be affected by the interlayer spacing and the size of the intercalated anion. In order to overcome the low adsorption capacity, various efforts had been made to modify their structures, including inserting organic anions between layers (Wang et al., 2012; Sakr et al., 2018), incorporating doping elements such as alkali metal ions (Choi et al., 2010; Li et al., 2017), and grafting amino groups to increase adsorption sites (Wang et al., 2012b; Ezeh et al., 2017). Lwin et al. (Lwin et al., 2009) comprehensively reported that the CO_2 adsorption capacity was dependent on temperature, layer charge density, interlayer spacing, intercalated anionic species, and the stability of skeletal structure. The layered structure are related to the type and mole ratio of M^{2+} and M^{3+}metal atoms. However, the intrinsic link between CO_2 adsorption capacity and cation composition is not clear. The atomic or electric state of the lamellae could not easily be determined by experimental measurements, so the quantum chemistry calculations should be useful as a supplement (Pu et al., 2008).

In this work, A series of LDHs (Mg-Al-LDH, Ca-Al-LDH, Zn-Al-LDH, Mg-Fe-LDH) intercalated by sodium dodecyl sulfate samples have been synthesized with co-precipitation method. The influences of the metal cation species of M^{2+} and M^{3+} on the CO_2 adsorption capacity was studied.

2. Experimental

2.1. Preparation of LDH intercalated by sodium dodecyl sulfate

The sodium dodecyl sulfate intercalated Mg-Al-LDH, Ca-Al-LDH, Zn-Al-LDH and Mg-Fe-LDH were synthesized by a co-precipitation method. Solution A was prepared by dissolving M^{2+} and M^{3+}

metal nitrate salts with mole ratio of 3:1 in 50 ml distilled water. The four different solutions A were Mg-Al, Ca-Al, Zn-Al and Mg-Fe nitrate solutions with an equal molar concentration of metal cations. Solution B was prepared by dissolving 3 g sodium dodecyl sulfate in 100 ml distilled water. Then the solution A was added to solution B under vigorous stirring at moderate rate in 70°C water bath. The pH value of the mixture was keep at 10 (± 0.1) by adding 1M NaOH solution. The mixture was aged for 4 h by stirring at constant temperature. Then the precipitation was filtered, washed with distilled water and dried at 70°C overnight.

2.2. Characterization of the samples

Elemental analysis was performed by a PE 2400 Series II CHNS/O Elemental Analyzer. The carbon, hydrogen, nitrogen and sulfur weight were detected. Approximately 1.5 mg sample was sealed in tin capsules without air. The blank and standard (acetanilide) were detected until the k-factor was stabled. The k-factor values of 16.5 ±3.5 for carbon, 50 ± 20 for hydrogen and 6.0±3.0 for nitrogen.

XRD was using a X'Pert PRO powder diffractometer with scanning range from 2-65°. The internal spacing was determined by the d_{003} peaks by XRD.

N_2 adsorption and desorption were measured at -196°C in liquid nitrogen by an ASAP2020 adsorption instrument. The specific surface was calculated by BET equations. The pore size distribution was calculated by BJH method.

CO2 temperature programmed desorption (CO_2-TPD) analysis was conducted using AutoChem II 2920. The TPD of CO_2 measurements were conducted to evaluate the basicity of the catalysts. 0.1 g of the adsorbent was treated in the reactor in Ar atmosphere at 140°C for 30 min.

CO_2 adsorption was performed by Tarsus F3 TG209 thermogravimetric analyzer. Approximately 10

mg sample was heated from 30°C to 140°C at 25°C/min under N_2 atmosphene. The sample was maintained at 140°C for 30 min and then cooled to 30°C at 15 °C/min. The sample was kept at 30°C for 30 min. After that, the N_2 atmosphene was converted to CO_2 atmosphene. Then CO_2 adsorption was held for 90 min. The CO_2 adsorption capacity of the sample was determined by the mass changes .

2.3. Computational method

The cluster models of the lamellae were established as reported (Lwin and Abdullah, 2009). The models were fully geometric optimized by density functional theory at the level of B3PW91/Lanl2DZ. The quantum chemical calculation work was done by Gaussian 03 software program package.

3. Results and discussion

3.1. Characterization results of the samples

The results of elemental analysis and XRD are shown in Table 1. In the interlayer of the samples, the intercalated anions are nitrate ion (NO_3^-) and carbonate ion (CO_3^{2-}). The nitrate ions come from metal nitrate salts. The carbonate ions come from the CO_2 in the atmosphere and the distilled water. The content of the intercalated anions are calculated based on weight percentage of the carbon, hydrogen, nitrogen and sulfur. The results are closed to the values reported before (Wang et al., 2012a) for the sodium dodecyl sulfate intercalated Mg-Al LDH, which had 1.87 mmol/g dodecyl sulfate, 0.12 mmol/g nitrate and 1.04 mmol/g carbonate.

Fig. 1 shows the XRD patterns of the sodium dodecyl sulfate intercalated LDHs. Samples Mg-Al-SDS-LDH, Ca-Al-SDS-LDH and Zn-Al-SDS-LDH have similar XRD patterns with the characteristic (003), and (006) peaks of LDH in the low angle region. It proves that the sodium dodecyl sulfate intercalated LDHs were successfully synthesized. The interlayer

spacing of the LDH samples was increased compared to the Mg-Al-CO_3-LDH (0.76 nm) (Cavani et al., 1991). Mg-Fe-SDS-LDH has low intensity (003) and (006) reflections, indicating the less ordered structure compared with the other three samples. The nitrogen adsorption results (Table 2) show that Mg-Al-SDS-LDH, Ca-Al-SDS-LDH and Zn-Al-SDS-LDH have low surface area of 1-4 m^2/g, while Mg-Fe-SDS-LDH has a relatively high surface area of 20 m^2/g. It can be explained as that: Fe^{3+} in the Mg-Fe-SDS-LDH has a Jahn-Teller effect in its six-coordinates, which decreases the stability of the system, therefore the peaks of (003) and (006) of XRD are weakened, and the specific surface area of the material increases significantly because of the structural distortion.

3.2. CO_2 adsorption

A typical TGA curve with three main stages (0-35, 35-72 and 72-162 min) for CO_2 adsorption measurement of Mg-Al-SDS-LDH is shown in Fig. 2. The stage I was from 30 to 140°C with a total weight loss of 8.53%, which was attributed to the removal of the adsorbed CO_2 and the water on the surface and in the interlayer (Wang et al., 2012a). At this stage the total weight loss of 9.62% , 16.6% and 5.98% is for Ca-Al-SDS-LDH, Zn-Al-SDS-LDH and Mg-Fe-SDS-LDH respectively. At stage II, the sample was cooled to 30°C and had a weight gain before the CO_2 adsorption. The weight gain can be attributed to a slight amount of CO_2 and H_2O adsorption in the pipe. At stage III, the CO_2 gas was inputted and the sample started to adsorb CO_2 molecules.

Fig. 3 shows the CO_2 adsorption curves for sodium dodecyl sulfate intercalated LDHs. Ca-Al-SDS-LDH has a maximum CO_2 adsorption capacity of 0.58mmol/g, Mg-Al-SDS-LDH has a moderate value of 0.45mmol/g, while Zn-Al-SDS-LDH has a minimum CO_2 adsorption capacity of 0.35mmol/g, it means that the CO_2 adsorption capacity varies with the change of M^{2+},obviously. When

Al atom is replaced by Fe atom, the CO_2 adsorption capacity is decreased. The sample of Mg-Fe-SDS-LDH has the highest adsorption rate at the first 10 minutes, then keeps the CO_2 adsorption capacity around 0.37mmol/g . In addition, the adsorption curves of Ca-Al-SDS-LDH, MgAl-SDS-LDH and Zn-Al-SDS-LDH are all of the Freundlich type, while only Mg-Fe-SDS-LDH is of the Langmuir type, which is attributed to its different basic sites (Fig. 4). In the CO_2-TPD diagram, the peak (<100°C) is interpreted as physical adsorption, and the physical desorption peak of Mg-Fe-SDS-LDH is relatively large because of the large specific surface area. Since the dehydroxylation reaction begins to occur at about 200°C, and the desorption peak above 200°C is derived from the decomposition of CO_3^{2-} or HCO_3^- between the layers, which also indicates that some of the CO_2 reacts with the hydroxyl groups on the layer. The significantly larger desorption peak is also consistent with the a larger adsorption capacity (Ishihara et al., 2013). Ca-Al-SDS-LDH has a weakly basic site at 125°C. The peak of Mg-Fe-SDS-LDH overlaps with the physical desorption peak, which may be the higher adsorption rate of Mg-Fe-SDS-LDH in the first 10 min.

3.3. Quantum chemistry calculations

Fig. 5 shows the structure of cluster model for Mg-Al LDH, which has the formula of $[Mg_6Al(OH)_{12}]^{3+}$. The other cluster models can be established by replacing the Mg and Al atoms with Ca, Zn and Fe atoms. Table 3 shows the bond length between metal and oxygen atoms in the model. The Ca—O bond length of $[Ca_6Al(OH)_{12}]^{3+}$ is the longest in the model, and the pore size of Ca-Al-SDS-LDH sample is the biggest (Table 2). The Mg—O bond length of $[Mg_6Fe(OH)_{12}]^{3+}$ is the shortest, and the pore size of the sample Mg-Fe-SDS-LDH is the smallest (Table 2). Although the M^{3+}—O bond length of the model is different, It indicated that the pore size is most possibly determined by the bond length of M^{2+}—O.

To investigate the relationship between layered structure and CO_2 adsorption, electronic properties of cluster models were discussed. Hydrogen bond can be described as O—H…O, the hydroxyl group was a proton donator and oxygen is a proton accepter (Grabowski, 2004). Layered structure has hydroxyl groups, which can form hydrogen bond with CO_2 and increase the CO_2 adsorption. The hydroxyl groups of water in the interlayers of LDH, also can affect the CO_2 adsorption, therefore, it was removed before the CO_2 adsorption measurement (at Stage I in Fig.2). According to Frontier's orbital theory, Lowest Unoccupied Molecular Orbital (LUMO) of proton donator and Highest Occupied Molecular Orbital (HOMO) of proton accepter were frequently considered (Fukui, 1982; Kandemirli and Sagdinc, 2007). It is more probable to accept electrons with the lower the values of E_{LUMO},and it is easier to form hydrogen bond with the smaller the value of ΔE (Li et al., 2007). From the Table 4, the value of E_{LUMO} of LDH model is $[Zn_6Al(OH)_{12}]^{3+}$ < $[Mg_6Al(OH)_{12}]^{3+}$ < $[Ca_6Al(OH)_{12}]^{3+}$ and $[Mg_6Fe(OH)_{12}]^{3+}$ < $[Mg_6Al(OH)_{12}]^{3+}$, which is opposite to the result of CO_2 absorption (Fig. 3). The ΔE of $[Mg_6Al(OH)_{12}]^{3+}$ with CO_2 is smallest, it mesns that the LUMO orbital of $[Mg_6Fe(OH)_{12}]^{3+}$ is most easily to accept electrons. However, the CO_2 adsorption capacity of Ca-Al-SDS-LDH is the highest (Fig. 3), it means that the CO_2 adsorption capacity of samples have no clearly relationship with ΔE*, and* has an *opposite* relationship with E_{LUMO} in experiment. The Mulliken charges distribution of the cluster models is given in Table 5. The H atom of Ca-Al-SDS-LDH has the least charges, and has a highest CO_2 adsorption, The LUMO orbital density distributions of the cluster models are shown in Fig. 5. The densities of LUMO orbital are followed in an order of $[Ca_6Al(OH)_{12}]^{3+}$ > $[Mg_6Al(OH)_{12}]^{3+}$ > $[Zn_6Al(OH)_{12}]^{3+}$ and $[Mg_6Al(OH)_{12}]^{3+}$ > $[Mg_6Fe(OH)_{12}]^{3+}$. The HOMO and LUMO orbital densities could be used to determine the chemical reactivity of the molecule site (Kohn et al., 1996). The higher density of LUMO orbital is, the more easily O—H…O hydrogen bond can form. This can be used to explain the CO_2

adsorption capacity of materials in the experiment. Therefore, the CO_2 adsorption capacity of materials is correlated to the value of E_{LUMO} and the density of LUMO orbital.

4. Conclusions

Sodium dodecyl sulfate intercalated LDHs had been synthesized by coprecipitation method and studied as CO_2 adsorbents at 30°C under 1 bar. These materials were characterized by elemental analysis, XRD, N_2 physical adsorption and desorption and B3PW91/Lanl2DZ methods, and the results showed that the trivalent cation species had a great influence on the crystal phases and the pore structures of LDHs. Ca-Al-SDS-LDH had a maximum CO_2 adsorption capacity of 0.58 mmol/g, and Zn-Al-SDS-LDH had a minimum CO_2 adsorption capacity of 0.35mmol/g. CO_2 adsorption capacity of LDHs was significantly affected by the value of E_{LUMO} and the density of LUMO orbital, and the higher E_{LUMO} and density of LUMO orbital leaded to higher CO_2 adsorption capacity.

Acknowledgments

The work was supported by the Open Project Program of the State Key Laboratory of Chemical Engineering (SKL-ChE-11A02), Zhejiang Provincial Middle-aged Subject Leaders Project (pd2013011) and Ningbo Bureau of Science and Technology (Grant No. 2012B10042).

References:

Aschenbrenner, O., McGuire, P., Alsamaq, S., Wang, J., Supasitmongkol, S., Al-Duri, B., Styring, P., Wood. J., 2011. Adsorption of carbon dioxide on hydrotalcite-like compounds of different compositions. Chem. Eng. Res. Des. 89, 1711-1721.

Bergaya, F., Theng, B.K.G. and Lagaly, G.(Eds.), 2006. Handbook of Clay Science. Elsevier Science, Oxford 1021-1095.

193 Cavani, F., Trifirò, F., Vaccari, A., 1991. Hydrotalcite-type anionic clays: Preparation, properties and
194 applications. Catal. Today 11, 173-301.
195 Choi, S., Drese, J.H., Jones, C.W., 2010. Adsorbent Materials for Carbon Dioxide Capture from Large
196 Anthropogenic Point Sources. ChemSusChem. 2(9), 796-854.
197 Ezeh, C.I., Tomatis, M., Yang, X., He, J., Sun, C.G., 2017. Ultrasonic and Hydrothermal Mediated
198 Synthesis Routes for Functionalized Mg-Al LDH: Comparison Study on Surface Morphology,
199 Basic Site Strength, Cyclic Sorption Efficiency and Effectiveness. Ultrason Sonochem. 40, 341.
200 Fukui, K., 1982. Role of frontier orbitals in chemical reactions. *Science* 218(4575), 747-754.
201 Grabowski, S.J., 2004. Hydrogen bonding strength—measures based on geometric and topological
202 parameters. J. Phys. Org. Chem. 17(1), 18-31.
203 Hudson, M.R., Queen, W.L., Mason, J.A., Fickel, D.W., Lobo, R.F., Brown, C.M., 2012. Unconventional,
204 Highly Selective CO_2 Adsorption in Zeolite SSZ-13. J. Am. Chem. Soc. 134, 1970-1973.
205 Hutson, N.D. and Attwood, B.C., 2008. High temperature adsorption of CO_2 on various hydrotalcite-like
206 compound. Adsorption 14, 781-789.
207 Ishihara, S., Sahoo, P., Deguchi, K., Ohki, S., Tansho, M., Shimizu, T., Labuta, J., Hill, J.P., Ariga, K.,
208 Watanabe, K., Yamauchi, Y., Suehara, S., Iyi, N., 2013. Dynamic Breathing of CO_2 by Hydrotalcite.
209 J. Am. Chem. Soc. 135(48), 18040-18043.
210 Kandemirli, F. and Sagdinc, S.,2007. Theoretical study of corrosion inhibition of amides and
211 thiosemicarbazones. Corros. Sci. 49(5), 2118-2130.
212 Kohn, W., Becke, A.D., Parr, R.G.,1996. Density Functional Theory of Electronic Structure. *J. Phys.*
213 *Chem.* 100(31), 12974-12980.

Li, S., Shi, Y., Zheng, H., Cai, N., 2017. Development of carboxyl-layered double hydrotalcites of enhanced CO_2 capture capacity by K_2CO_3 promotion. Adsorption 23, 239-248.

Li, W., He, Q., Pei, C., Hou B., 2007. Experimental and theoretical investigation of the adsorption behaviour of new triazole derivatives as inhibitors for mild steel corrosion in acid media. Electrochim Acta. 52(22), 6386-6394.

Liu, F.Q., Li, W.H., Liu, B.C., Li, R.X., 2013. Synthesis, characterization, and high temperature CO_2 capture of new CaO based hollow sphere sorbents. J. Mater. Chem. A 1(27), 8037-8044.

Lwin, Y. and Abdullah, F., 2009. High temperature adsorption of carbon dioxide on Cu–Al hydrotalcite-derived mixed oxides: kinetics and equilibria by thermogravimetry. J. Therm. Anal. Calorim. 97(3), 885-889.

Oliveira, T.G., Souza, M.J.B., Coriolano, A.C.F., Pedrosa, A.M.G., Araujo, A.S.,2018. CO_2 adsorption on systems involving ethylenediamine impregnated on nanoporous materials. Petroleum Science and Technology 36(23), 1977-1982.

Plaza, M.G., Pevida, C., Martín, C.F., Fermoso, J., Pis, J.J., Rubiera, F., 2010. Developing almond shell-derived activated carbons as CO_2 adsorbents. Sep. Purif. Technol. 71, 102-106.

Pu, M., Wang, Y.L., Liu, L.Y., Liu, Y.H., He, J., 2008. Evans, D.G. Quantum chemistry and molecular mechanics studies of the lamella structure of hydrotalcite with Mg/Al ratio of 3. J. Phys. Chem. Solids 69(5), 1066-1069.

Reddy, M.K.R., Xu, Z.P., Costa, J.C.D.D., 2008. Influence of Water on High-Temperature CO_2 Capture Using Layered Double Hydroxide Derivatives. Ind. Eng. Chem. Res. 47(8), 2630-2635.

Sakr A.A., Zaki T., Elgabry O., 2018. Mg-Zn-Al LDH: Influence of intercalated anions on CO_2 removal from natural gas. Applied Clay Science 160,263-269.

Sharma, U., Tyagi, B., Jasra, R.V., 2008. Synthesis and Characterization of Mg−Al−CO_3 Layered Double Hydroxide for CO_2 Adsorption. *Ind. Eng. Chem. Res.* 47(23), 9588-9595.

Torres-Rodríguez, D.A., Lima, E., Valente, J.S., Pfeiffer, H., 2011. CO_2 capture at low temperatures (30-80°C) and in the presence of water vapor over a thermally activated Mg-Al layered double hydroxide. *J. Phys. Chem. A*. 115(44) , 12243-12250.

Wang, J., Stevens, L.A., Drage, T.C., Wood, J., 2012a. Preparation and CO_2 adsorption of amine modified Mg–Al LDH via exfoliation route. *Chem. Eng. Sci.* 68(1), 424-431.

Wang, J., Stevens, L.A., Drage, T.C., Snape, C.E., Wood, J., 2012b. Preparation and CO_2 adsorption of amine modified layered double hydroxide via anionic surfactant-mediated route. *Chem. Eng. J.* 181-182(2), 267-275.

Wang, X.P., Yu, J.J., Cheng, J., Hao, Z.P., Xu, Z.P., 2008. High-Temperature Adsorption of Carbon Dioxide on Mixed Oxides Derived from Hydrotalcite-Like Compounds. *Environ. Sci. Technol.* 42(2), 614-618 .

Wang, Q., Hui, H.T., Zhong, Z., Luo, J., Borgna, A., 2012. Synthesis of high-temperature CO_2 adsorbents from organo-layered double hydroxides with markedly improved CO_2 capture capacity. Energ Environ. Sci. 5(6), 7526-7530.

Wang, Q., Wu, Z., Tay, H.H., Chen, L., Liu, Y., Chang, J., Zhong, Z., Luo, J., Borgna, A., 2011. High temperature adsorption of CO_2 on Mg–Al hydrotalcite: Effect of the charge compensating anions and the synthesis pH. Catal. Today 164(1), 198-203.

Ye, L. and Abdullah, F., 2009. High temperature adsorption of carbon dioxide on Cu–Al hydrotalcite-derived mixed oxides: kinetics and equilibria by thermogravimetry. J. Therm Anal Calorim. 97(3), 885-889.

Zhao, H., Yan, W., Bian, Z., Hu, J., Liu, H., 2012. Investigation of Mg modified mesoporous silicas and their CO_2 adsorption capacities. Solid State Sci. 14, 250-257.

Zou, Y., Mata, A.V., Rodrigues, A.E., 2001. Adsorption of Carbon Dioxide onto Hydrotalcite-like Compounds (HTlcs) at High Temperatures. Ind. Eng. Chem. Res. 40(1), 204-209.

265 **Fig. 1.** XRD patterns for sodium dodecyl sulfate intercalated LDHs.

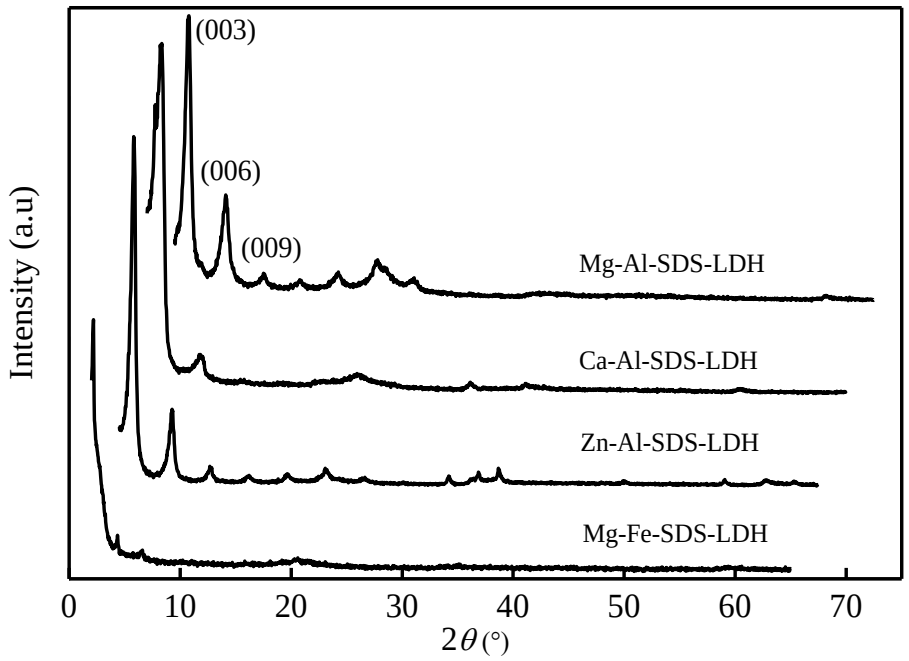

266

Fig. 2. A typical TGA curve for CO_2 adsorption measurement of Mg-Al-SDS-LDH.

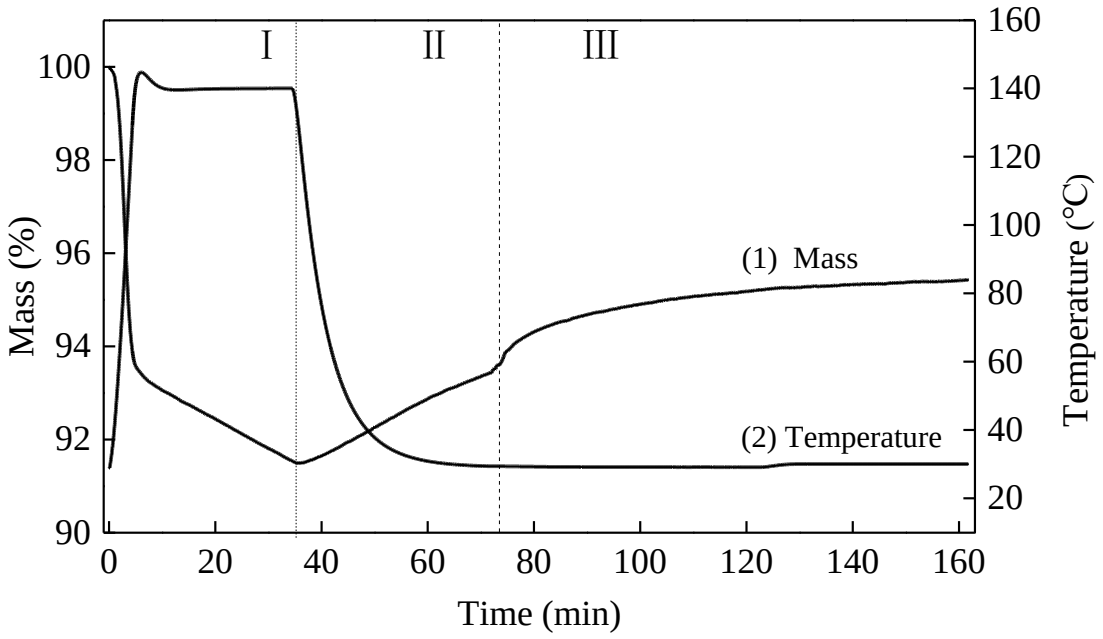

272

273 **Fig. 3.** CO_2 amount adsorbed curves for sodium dodecyl sulfate intercalated LDHs.

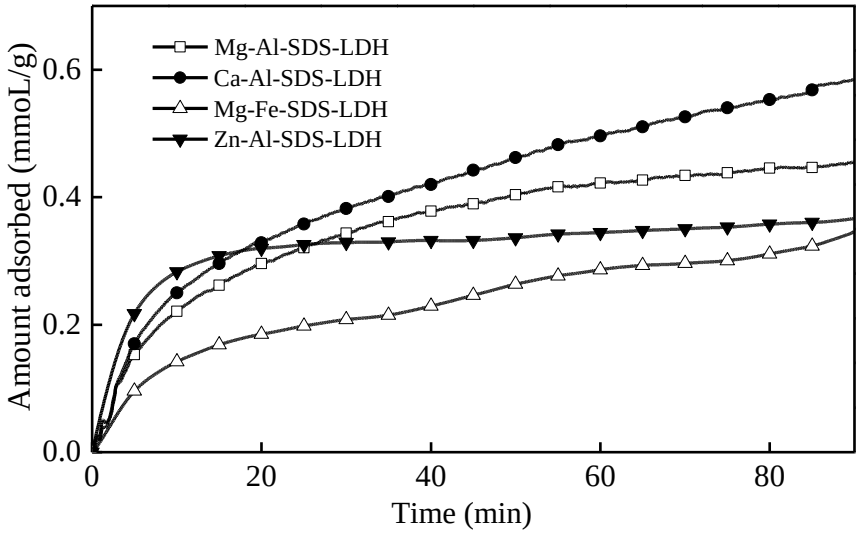

274

275

276 **Fig. 4.** The CO_2-TPD of Ca-Al-SDS-LDH and Me-Fe-SDS-LDH

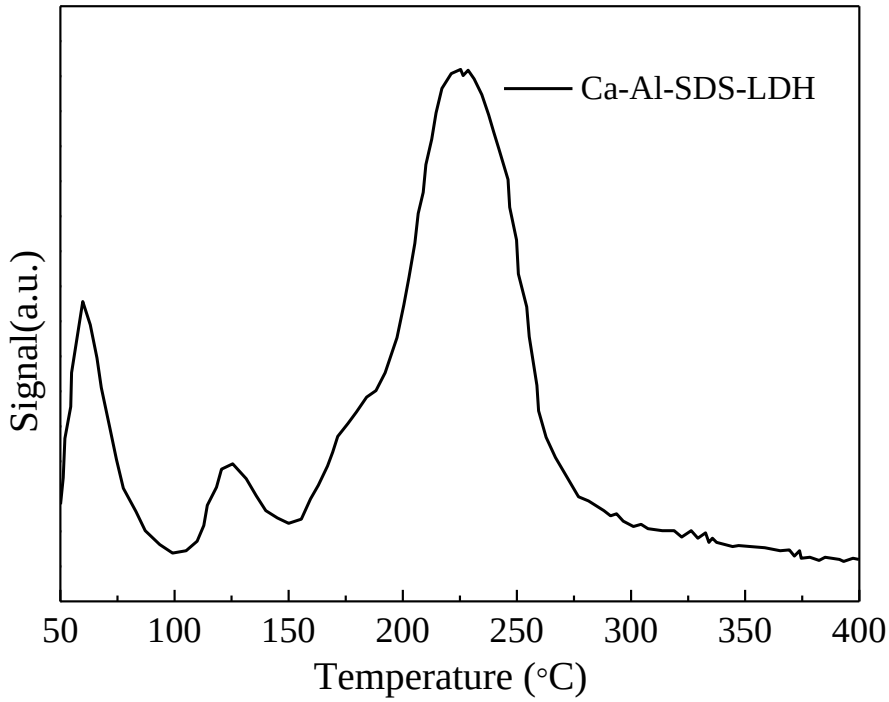

277

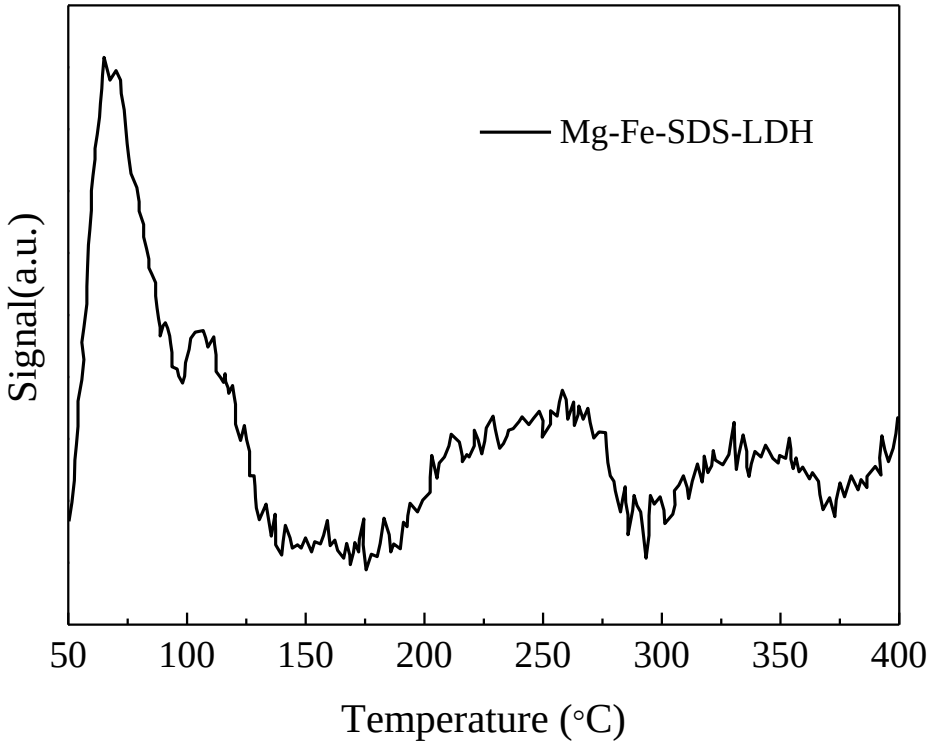

278

279

Fig. 5. The structure of cluster model for Mg-Al LDH.

White: hydrogen, Red: oxygen, Yellow: Mg, Pink: Al

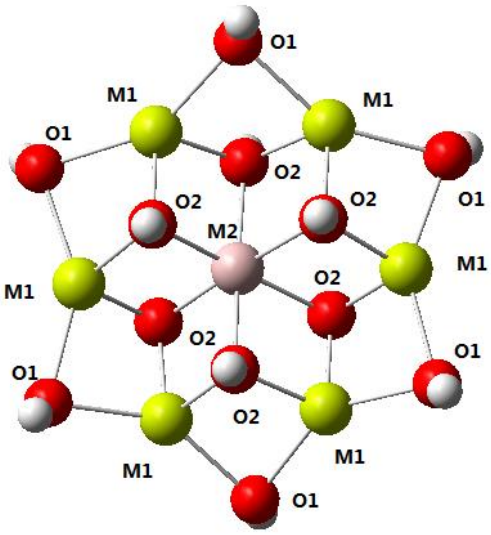

Fig. 6. The LUMO orbital spatial distributions of cluster models.

(a) $[Mg_6Al(OH)_{12}]^{3+}$, (b) $[Ca_6Al(OH)_{12}]^{3+}$, (c) $[Zn_6Al(OH)_{12}]^{3+}$ and (d) $[Mg_6Fe(OH)_{12}]^{3+}$

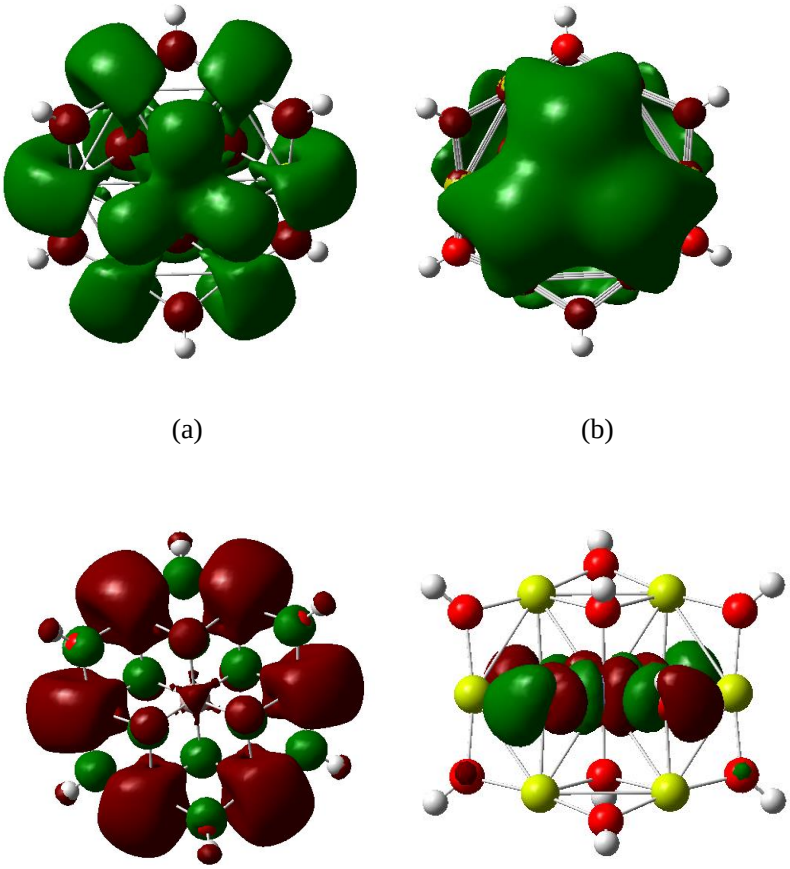

(a) (b)

(c) (d)

292 **Table 1.** Results of elemental analysis and XRD

Sample	Elemental weight (%)				Formula for intercalated molecules (mmol/g)	Interlayer spacing(nm)
	C	H	N	S		
Mg-Al-SDS-LDH	31.64	8.09	0.09	6.42	$(C_{12}H_{25}SO_4^-)_{2.01}(NO_3^-)_{0.064}\ (CO_3^{2-})_{2.25}$	2.89
Ca-Al-SDS-LDH	31.13	7.90	0.12	5.48	$(C_{12}H_{25}SO_4^-)_{1.71}(NO_3^-)_{0.086}(CO_3^{2-})_{5.42}$	2.41
Zn-Al-SDS-LDH	23.42	6.25	0.07	4.80	$(C_{12}H_{25}SO_4^-)_{1.50}(NO_3^-)_{0.050}\ (CO_3^{2-})_{1.52}$	2.51
Mg-Fe-SDS-LDH	29.21	7.45	0.29	5.58	$(C_{12}H_{25}SO_4^-)_{1.74}(NO_3^-)_{0.207}\ (CO_3^{2-})_{3.46}$	2.81

293

294 **Table 2.** Results of Nitrogen adsorption and desorption at lower temperature

Sample	A_p/(m^2 g ^{1})	r_p/(nm)	V_p/(cm^3 g ^{1})
Mg-Al-SDS-LDH	4.34	7.93	8.60×10^{-3}
Ca-Al-SDS-LDH	0.92	48.00	1.10×10^{-2}
Zn-Al-SDS-LDH	3.42	26.00	2.22×10^{-2}
Mg-Fe-SDS-LDH	19.66	3.27	1.61×10^{-2}

295

296 **Table 3.** Bond length between metal and oxygen of the model

Model	M^{2+}—O_{in}(Å)	M^{2+}—O_{out}(Å)	M^{3+}—O(Å)
$[Mg_6Al(OH)_{12}]^{3+}$	2.087	1.945	1.926
$[Ca_6Al(OH)_{12}]^{3+}$	2.465	2.247	1.973
$[Zn_6Al(OH)_{12}]^{3+}$	2.135	1.951	1.925
$[Mg_6Fe(OH)_{12}]^{3+}$	2.077	1.939	1.934

297 In: stands for the atoms in the centre of the model, and out: stands for the atoms around the model.

298

299 **Table 4.** Calculated energy levels, ELUMO, EHOMO of the cluster models and CO2 molecule and ΔE

	$[Mg_6Al(OH)_{12}]^{3+}$	$[Ca_6Al(OH)_{12}]^{3+}$	$[Zn_6Al(OH)_{12}]^{3+}$	$[Mg_6Fe(OH)_{12}]^{3+}$		CO_2
				α orbital	β orbital	
LUMO(a.u.)	-0.37254	-0.34089	-0.40857	-0.46900	-0.64770	-0.01271
HOMO(a.u.)	-0.64558	-0.57191	-0.65370	-0.48521	-0.64365	-0.38136
Δ*E*(a.u.)	-0.00882	-0.04047	0.02721	0.08764	0.26634	-

300 ΔE is equaled to the energy gap between E_{LUMO} of the cluster models and E_{HOMO} of the CO_2 molecule
301

302 **Table 5.** Mulliken charges distribution of the cluster models (a.u.)

Model	H1	H2	O1	O2	M1	M2
$Mg_6Al(OH)_{12}^{3+}$	0.455	0.462	-1.052	-1.082	1.366	2.107
$Ca_6Al(OH)_{12}^{3+}$	0.425	0.415	-1.172	-1.078	1.634	1.654
$Zn_6Al(OH)_{12}^{3+}$	0.458	0.457	-0.981	-1.019	1.285	1.797
$Mg_6Fe(OH)_{12}^{3+}$	0.457	0.452	-1.056	-0.906	1.466	0.551

303

304

305